nature communications

Article

https://doi.org/10.1038/s41467-026-71842-w

Layer-specific attentional modulation in the human primary somatosensory cortex

Received: 27 December 2024

Accepted: 29 March 2026

Published online: 13 April 2026

Check for updates

Dongho Kim[1,2], SoHyun Han[3], Seongyun Kim[1], Seulgi Eun[4], Min-Suk Kang[1,2,5], Choong-Wan Woo[1,2,6,7] & Seong-Gi Kim[1,2,6]

Selective attention enhances relevant sensory inputs while filtering out distractions, yet its layer-specific effects remain poorly understood. Here, we used microvascular-specific spin-echo BOLD fMRI at 7 T to investigate attentional modulation across cortical layers in the human primary somatosensory cortex (S1) during finger and wrist stimulation. During passive, unattended stimulation, the middle and deep layers exhibited stronger signals than the superficial layer. In the attended finger region, attention significantly increased activity in the superficial layer, consistent with top-down feedback, and decreased activity in the deep layer, while leaving the middle layer unchanged. In the wrist region processing tactile or pain distractors, signals were uniformly suppressed across layers, including the thalamic-input middle layer, consistent with the impaired sensory discrimination observed in behavioral studies. Our findings reveal that attention reshapes laminar activation in S1, selectively enhancing relevant signals while suppressing irrelevant input, consistent with an attentional gating mechanism.

When navigating environments with a myriad of competing sensory inputs, selective attention allows individuals to focus on task-relevant stimuli while controlling distraction[1–9]. In the brain, the sensory cortex maps tactile inputs from the external environment onto topographically organized receptive fields[10], and attention modulates their responses by increasing the neural representation of relevant stimuli while reducing responses representing distractors[11–20]. Classic neurophysiological studies have demonstrated attentional modulation both in early sensory areas[4,21] and in higher-order regions involved in top-down control[22,23]. However, despite extensive evidence that attention modulates neural responses across multiple brain regions, much less is known about how such modulation is expressed within the cortical microcircuit. In particular, whether attention differentially influences the responses of specific cortical layers—thereby providing insight into how sensory information is processed in a layer-specific manner—remains unclear.

Attentional modulation in the human somatosensory cortex can be examined using high-resolution fMRI, focusing on laminar organization. Primary sensory cortices (e.g., V1 and S1) process sensory information through a multilayered structure: layer 4 receives initial sensory input from the thalamus, layers 2/3 integrate feedforward and feedback inputs, and layers 5/6 transmit processed information to other cortical and subcortical regions, contributing to motor control and thalamic modulation[10,11,24–31]. Previous studies have shown that attention enhances perception by differentially modulating neural responses across cortical layers, particularly by increasing responses in the superficial layer[32–34], reflecting the prioritization of sensory information relevant to ongoing tasks or environmental demands[35,36]. However, while attention reliably increases superficial-layer responses, its influence on other layers remains inconclusive[33,34,37–41], and it is unknown whether representations of unattended distractors are modulated differently across layers. Therefore, we hypothesized that

[1]Center for Neuroscience Imaging Research, Institute for Basic Science, Suwon, South Korea. [2]Department of Brain Science and Engineering, Sungkyunkwan University, Suwon, South Korea. [3]Center for Bio-imaging and Translational Research, Korea Basic Science Institute, Cheongju, South Korea. [4]Division of KM Science Research, Korea Institute of Oriental Medicine (KIOM), Daejeon, South Korea. [5]Department of Psychology, Sungkyunkwan University, Seoul, South Korea. [6]Department of Biomedical Engineering, Sungkyunkwan University, Suwon, South Korea. [7]Department of Intelligent Precision Healthcare Convergence, Sungkyunkwan University, Suwon, South Korea. e-mail: waniwoo@skku.edu; seonggikim@skku.edu

attention-related suppression would exhibit a laminar profile different from that of attentional enhancement, reflecting distinct layer-specific influences in attended versus unattended regions.

To test our hypothesis, we investigated layer-specific attentional modulation in the primary somatosensory cortex (S1) of 17 human participants using microvascular-specific spin-echo BOLD fMRI at 7 T. In our paradigm, attention was consistently directed to the fingers (target site), while the wrist (distractor site) was concurrently stimulated but unattended, enabling us to investigate somatotopically organized modulation of attended versus unattended representations within S1. Two sets of competing stimuli were presented concurrently at a target site (fingers) and a distractor site (wrist): (i) tactile stimulation to both sites, and (ii) tactile stimulation to the target site with painful thermal stimulation to the distractor site. In the attended condition, participants discriminated tactile frequencies at the target site while ignoring the distractor. In the passive condition, the same stimuli were presented, but participants simply experienced them without performing a task; here, the term "distractor" is used solely to denote the non-target site, irrespective of attentional demands.

We found that passive stimulation elicited greater BOLD signals in the middle (layers 4/5) and deep layers (layer 6) than in the superficial layer (layers 2/3) across both the finger and wrist representations in S1. When attention is directed to the fingers, however, superficial-layer activity increased while deep-layer activity decreased in the attended finger region. In contrast, the unattended wrist representation showed uniform suppression across all layers, consistent with the impaired sensory discrimination observed in a follow-up behavioral experiment. Together, these findings demonstrate that attention induces distinct, layer-specific modulation in human S1, highlighting that even early sensory processing is shaped by attentional influences across both spatial and laminar domains[3,7,8,34].

Results

Overall experimental design

To obtain laminar-dependent fMRI responses in S1 at 7 T, imaging slices were precisely positioned perpendicular to the central sulcus between the motor and sensory cortices[42–45] (Fig. 1a). We used spin-echo (SE) BOLD contrast because of its high sensitivity to microvascular signals, whereas conventional gradient-echo BOLD is more susceptible to macrovascular contributions that can bias responses across cortical layers[42,46,47]. High-resolution SE-BOLD data were acquired at 0.8 mm isotropic resolution (Fig. 1b), and S1 was identified using anatomical MRI (Fig. 1b).

We employed two experimental designs: i) tactile stimuli delivered to the fingers with concurrent tactile stimuli to the wrist (Experiment 1), and ii) tactile stimuli to the fingers combined with thermal stimuli to the wrist (Experiment 2). In Experiment 1, tactile stimulation was applied to the left index and middle fingers (target site) and the left wrist (distractor site) (Fig. 1c). Four tactile stimulators were used—two on the fingers and two on the wrist—each delivering vibration frequencies of either 3 Hz or 8 Hz (Fig. 1d). Frequencies were randomly varied across trials. Eight participants (Subjects 1–8; Group 1) initially completed Experiment 1, and additional eight participants (Subjects 10–17; Group 2) were later recruited to replicate the findings. In Experiment 2, tactile stimulation was applied to the same fingers (two stimulators), while a single thermal stimulator delivered heat to the wrist ($n = 9$, including the eight Group 1 participants from Experiment 1 plus one additional participant; Fig. 1e). Finger stimulation was identical to that in Experiment 1, while the wrist thermal stimulus was set to 44 °C to activate nociceptors[48,49], ensuring it was perceptibly salient and sufficiently distracting[50] (see Fig. 1f).

For both experiments, participants were instructed to either: i) remain awake and experience both stimulations (passive condition), or ii) concentrate on discriminating tactile frequency differences of stimulators on their fingers (attended condition) (Fig. 1d). To ensure the two conditions were matched in motor demands, no behavioral responses were collected. Instead, we verbally confirmed with participants between runs that they perceived both finger and wrist stimuli. In each fMRI run, 18 s of stimulation followed by 36 s of rest were repeated eight times. High-resolution spin-echo BOLD fMRI data were processed by averaging runs at the subject level, followed by laminar sampling procedures (see Methods for details).

Laminar boundaries in the finger and wrist regions defined by anatomy and functional activation

To assess fMRI signal changes between the passive and attended conditions, it was essential to compare responses in the attended finger region and the unattended wrist region. These regions were identified through two localization steps: (1) lateral boundaries were delineated using functional activation maps and anatomical landmarks, and (2) cortical-depth boundaries were defined from anatomical images.

Finger and wrist regions were identified using the traveling wave paradigm (Fig. 2a and Supplementary Fig. 1a, b). Fifteen of the 17 participants, including the 7 who participated in both experiments, completed this separate localizer session. In this paradigm, four sites on the left arm—the fingers, hand, wrist, and forearm—were sequentially stimulated every 10 s in either forward or reverse order, and neural responses were measured using conventional gradient-echo (GE) BOLD contrast[51] (see Supplementary Fig. 1a, b). Finger and wrist regions identified by the localizer were further refined using activation maps from both passive and attended conditions (Fig. 2b). In the passive condition, activation patterns were distributed around the hand knob area within S1. When attention was directed to the fingers, the number of activated voxels was markedly reduced (see also Supplementary Fig. 1c, d). The finger region of interest (ROI) was defined as the voxels activated in both passive and attended conditions, located lateral to the hand knob. Because significant activation was often absent medial to the hand knob during attended stimulation, the wrist ROI was further refined based on two criteria: (1) anatomical landmarks (hand knob), and (2) activation during the passive condition (Fig. 2b for multiple slices in one subject; Supplementary Fig. 2 for a representative slice in the other participants). For two participants without localizer data, finger and wrist ROIs were defined using anatomical landmarks and the aforementioned functional activation criteria. Consequently, medio–lateral (somatotopic) boundaries separating the finger and wrist ROIs were delineated along the cortical surface (white dashed lines in Fig. 2b and Supplementary Fig. 2).

Laminar boundaries were determined as follows. The cortical depth of area 3b (~2 mm thick) was defined using GE/SE BOLD ratio images (Fig. 2c), which allowed visualization of both the cerebrospinal fluid (CSF)–gray matter (GM) boundary and the GM–white matter (WM) boundary[46]. This cortical ROI was divided into 8 equivolume depth bins. To identify the middle cortical layer (layer 4), quantitative depth-dependent T_1 (qT_1) values from T_1-weighted anatomical images were analyzed[52] (Fig. 2d and Supplementary Fig. 3b–d). Based on qT_1 gradient analysis and previous literature[53,54], bins 1–2 were grouped as superficial (layers 2/3), bins 4–5 as middle (layers 4/5), and bins 7–8 as deep (layer 6). These laminar ROIs were then used to extract time courses for each subject.

Attentional modulation differently affects the targeted finger area and the non-targeted wrist area in S1

We first examined attentional modulation of the BOLD signal, averaged across cortical depth, along lateral-to-medial columnar strips within area 3b of S1 before investigating layer-dependent responses in the finger and wrist ROIs defined above (Fig. 3a for multiple slices in a representative subject and Supplementary Fig. 4a for a single slice

https://doi.org/10.1038/s41467-026-71842-w

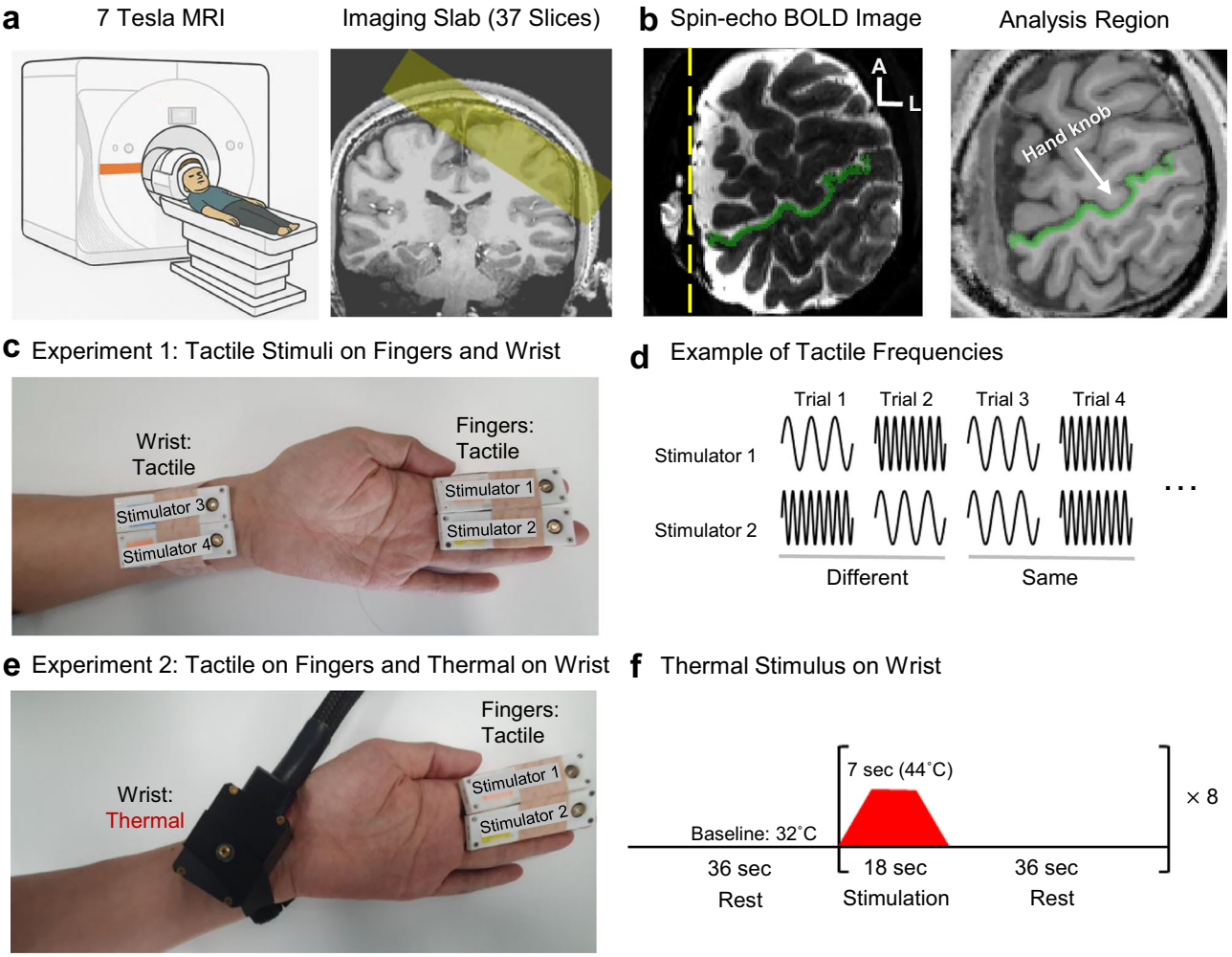

Fig. 1 | Research overview. a High-field (7 Tesla) MRI was used to acquire laminar-resolution fMRI data. Thirty-seven imaging slices were carefully positioned perpendicular to the central sulcus between the motor and somatosensory cortices to capture the S1 hand area. **b** Spin-echo BOLD imaging was performed with 0.8 mm isotropic resolution to detect layer-specific microvascular signals. The yellow dashed line marks the anatomical midline between the left and right hemispheres. Direction labels (A = anterior, L = lateral) indicate anatomical orientation within the slice. The right panel shows the anatomically defined analysis region along area 3b of S1 (green), with the hand knob marked for localization. **c** In Experiment 1, tactile stimuli were applied to the left index and middle fingers (task-relevant) and to the wrist (task-irrelevant distractors) for 18 s. Two stimulators were used for each site across eight functional runs, alternating between passive and attended conditions. **d** Example frequency patterns for the tactile stimuli. We independently manipulated the vibration frequency (3 Hz or 8 Hz) of each vibrator. In the attended condition, participants judged whether the two finger stimuli were the same or different in frequency, while ignoring the wrist stimulation. **e** In Experiment 2, the same tactile stimulation to the fingers was paired with a thermal stimulation to the wrist (replacing the wrist tactile distractor), introducing a more salient, nociceptive distractor. **f** Thermal stimulation protocol: heat increased from 32 °C baseline to 44 °C over ~5.5 s (2.18 °C/s), held for 7 s, then returned to baseline over the same rate. Each run began with a 36-s baseline, followed by 8 stimulation epochs (18 s each), each followed by a 36-s rest period.

across all sixteen participants in Experiment 1). The lateral-to-medial columnar strips were divided into five ROIs based on anatomical landmarks—particularly the hand knob—and somatotopic maps from the independent traveling-wave localizer (Fig. 3b). BOLD signal time courses (mean ± SEM, $n = 16$) were extracted from the five columnar ROIs during the passive and attended conditions in Experiment 1.

In the passive condition (Fig. 3b, left panel), responses were evident in Columns 2 and 3. When attention was directed to the fingers (right panel), the response in Column 2 increased, whereas that in Column 3 decreased markedly. This pattern was replicated in Experiment 2 (Supplementary Fig. 5a), indicating attentional enhancement in the finger-associated column ROI (Column 2) and suppression in the adjacent wrist-associated column ROI (Column 3). Our spatial activation profile matched predictions from the attention literature: in the passive condition, regions corresponding to both the stimulated fingers and wrist should show strong responses, whereas in the attended condition, the finger region should remain active but was suppressed in the wrist region and adjacent medial areas[1–9].

To quantify these effects, we computed the percent BOLD signal change within a window of 6–24 s after stimulus onset, chosen to capture the stimulation-evoked BOLD response while accounting for hemodynamic delay (Fig. 3c). A 2 (Condition: passive vs. attended) × 5 (Column: 1–5) repeated-measures ANOVA revealed a significant interaction (Experiment 1: $F(4, 60) = 3.082$, $p = 0.022$, partial $\eta^2 = 0.170$; Experiment 2: $F(4, 32) = 8.034$, $p < 0.001$, partial $\eta^2 = 0.501$), indicating that attention differentially modulated BOLD signals along the somatotopic axis, particularly between Columns 2 and 3 (Fig. 3c; see also Supplementary Fig. 4b, c for individual data points, and Supplementary Fig. 5b for the corresponding results in Experiment 2). These attentional effects across the somatotopic axis motivated us to test whether similar modulation occurs across cortical layers.

https://doi.org/10.1038/s41467-026-71842-w

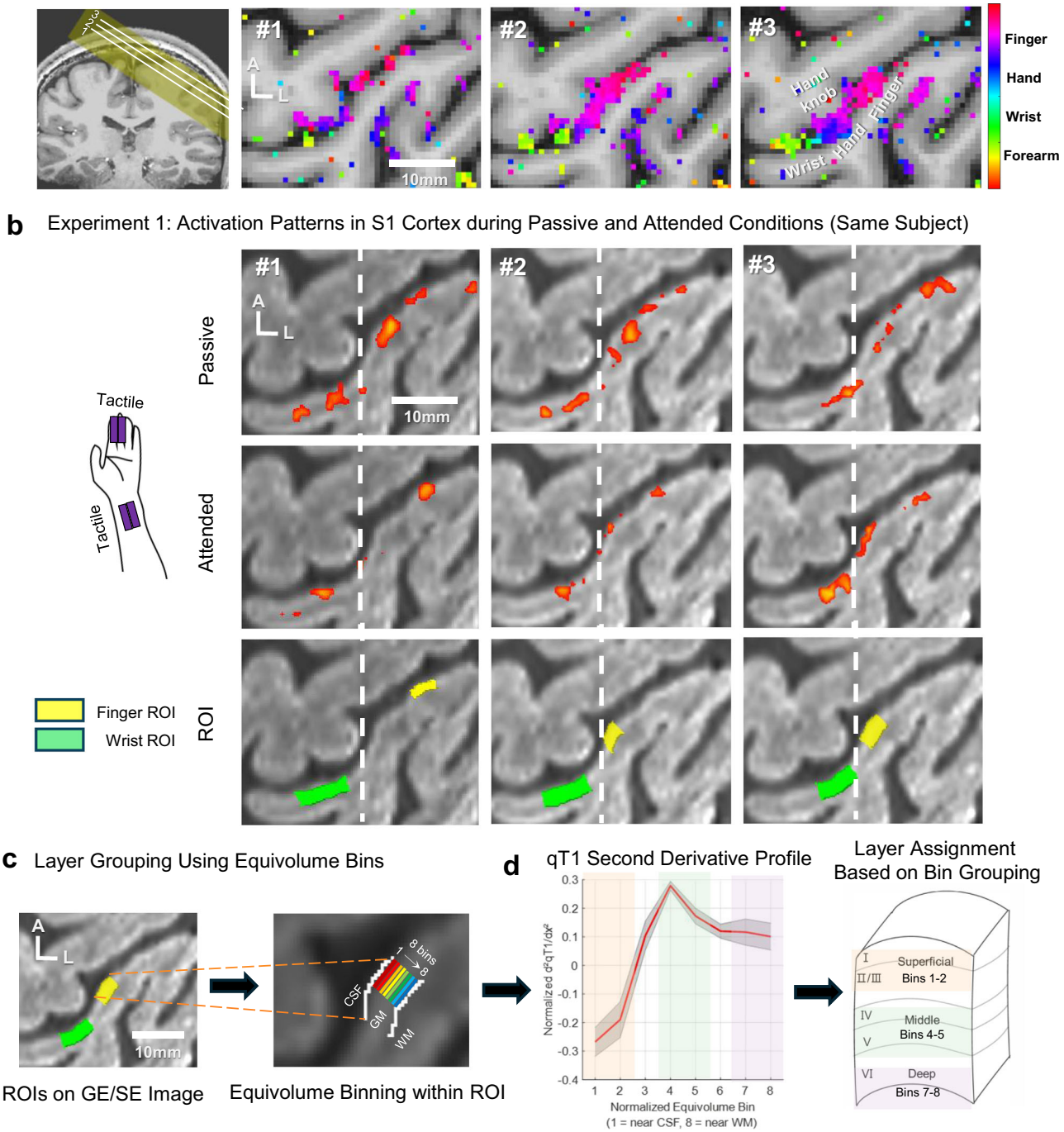

Fig. 2 | Laminar boundaries in finger and wrist regions defined by anatomical and functional activity. a Phase-encoded somatotopic maps across selected slices from a representative subject, centered on the hand knob. Colors denote peak locations for fingers (blue), hand (pink), wrist (green), and forearm (yellow). Slices were arranged from inferior to superior cortex. **b** Activation patterns during passive (top row) and attended (middle row) tactile stimulation in the same subject. Functional ROIs (bottom row) were defined based on activity patterns and anatomical landmarks: the finger ROI (yellow) includes voxels activated in both conditions lateral to the hand knob, while the wrist ROI (green) includes voxels activated only during passive stimulation, medial to the hand knob. **c** Functional ROIs were segmented along the cortical-depth axis into 8 equivolume bins using anatomical boundaries derived from GE/SE BOLD ratio image. **d** Second derivatives of quantitative T_1 (qT_1) profiles across cortical depth were used to assign laminar groups: superficial (Bins 1–2), middle (Bins 4–5), and deep (Bins 7–8), corresponding to classical cortical layers (see Supplementary Fig. 3). The peak of the qT_1 second derivative profile indicates the location of layer 4[52]. In our layer definition, layer 1 was not separately specified due to its low neuronal density and was included in the superficial layer.

Attention directed to the fingers modulates activity in the superficial and deep layers of the finger area, while suppressing activity in the entire wrist area

Next, we examined how attention modulates layer-dependent BOLD signals in S1 in Experiment 1. Because thalamic inputs primarily target the middle cortical layer, the middle layer is expected to exhibit the strongest BOLD response during passive tactile stimulation—assuming that SE-BOLD fMRI primarily reflects microvascular signals. The time courses in both the finger and wrist ROIs during the passive condition (Fig. 4a, b, left panels) showed that middle layer responses were

https://doi.org/10.1038/s41467-026-71842-w

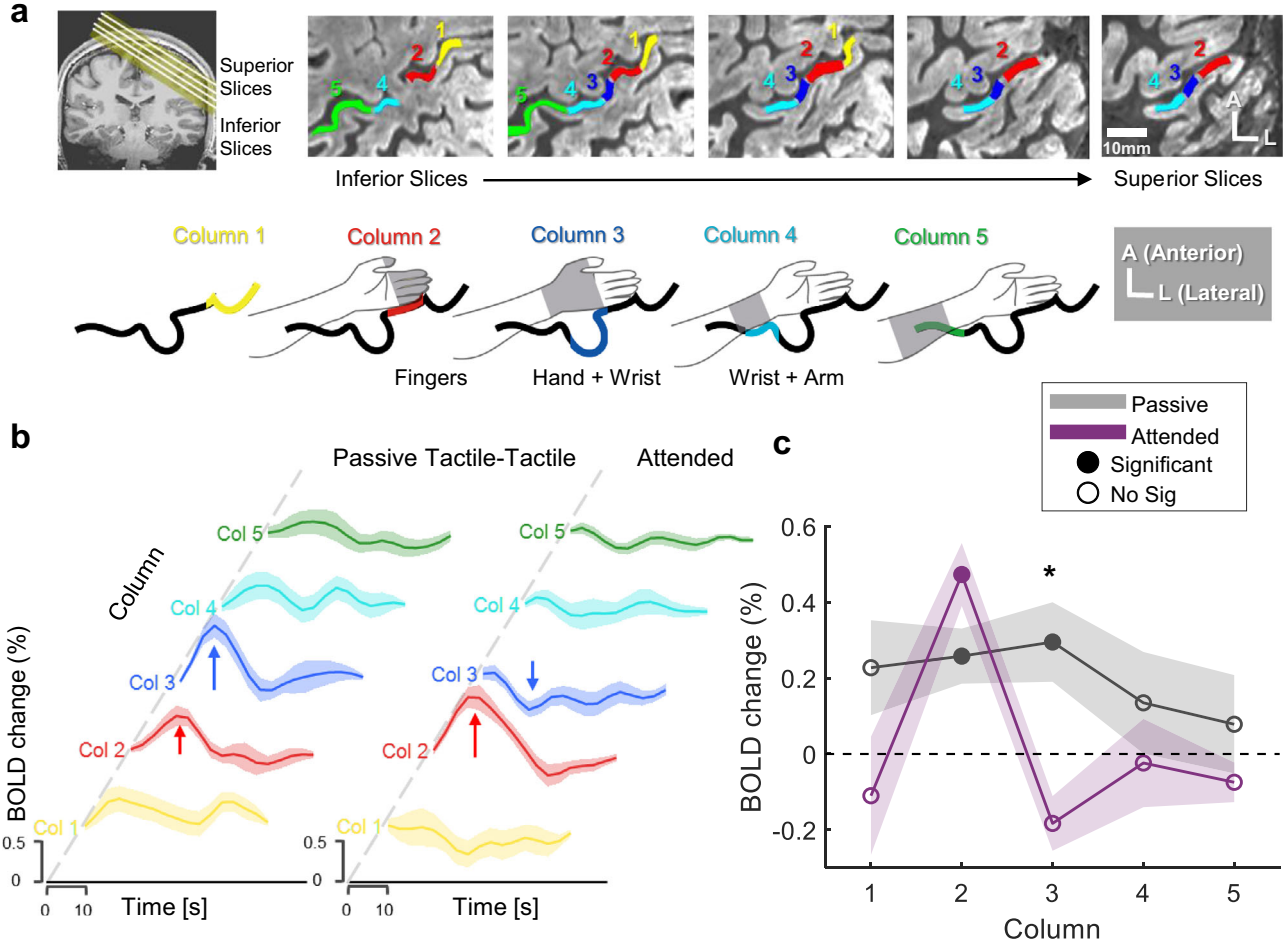

Fig. 3 | Attention-Modulated BOLD Signal Changes Across Columnar ROIs in S1. a Columnar ROIs were defined along the cortical ribbon of S1 using anatomical landmarks—particularly the hand knob—and refined with somatotopic maps from an independent traveling wave (TW) localizer that delivered cyclic tactile stimulation to the fingers and wrist. This ensured consistent yet individualized ROI placement. The top row displays SE-BOLD slices with GE/SE ratio image. Five columnar ROIs (Cols 1–5, colored yellow to green) trace a somatotopic gradient from the finger representation (Col 2) to the wrist representation (Col 3), with adjacent ROIs (Cols 1, 4, and 5) covering neighboring sensory areas. Note that the outermost ROIs taper in superior slices due to cortical narrowing. Schematic illustrations depict the approximate body region represented by each ROI, informed by the TW localizer. Orientation labels "A" (anterior) and "L" (lateral) indicate anatomical directions. **b** Time courses of BOLD signals for each columnar ROI during passive (left) and attended (right) conditions in Experiment 1 (mean ± SEM, $n = 16$). Arrows highlight attention-related modulation: Column 2 (red arrow) shows increased activation with attention, while Column 3 (blue arrow) shows decreased activation. **c** Average percent BOLD signal change during stimulation (18 s; see *Methods* for details on the averaging window) for each columnar ROI defined in (**a**). Under passive stimulation, Columns 2 and 3 showed significant activation relative to baseline (filled circles, FDR-corrected $q < 0.05$, one-sample t-test). During attention, Column 2 showed greater activation than during passive stimulation, although this effect did not survive FDR correction across columns (raw $p < 0.05$, FDR-corrected $q = 0.052$, paired t-test), whereas Column 3 exhibited strong attentional suppression (FDR-corrected $q < 0.05$, paired t-test). Filled circles indicate columns showing significant activation relative to baseline after correcting for multiple comparisons across the five columns within each condition using the Benjamini–Hochberg FDR procedure ($q < 0.05$). These condition-dependent effects corroborate the temporal dynamics observed in (**b**). Asterisks mark significant condition differences after FDR correction across the five columns (paired t-test: $^*q < 0.05$). In this and all subsequent figures, significance markers indicate only results surviving Benjamini–Hochberg FDR correction. Exact raw p values and corresponding FDR-adjusted q-values are provided in Supplementary Table S1. Shaded areas in (**b**, **c**) indicate ± SEM across participants ($n = 16$).

slightly higher than or comparable to those in the deep layer, and substantially greater than those in the superficial layer. Notably, prior GE-BOLD studies typically revealed greater middle-layer activation only after applying subtractive contrasts between conditions (e.g., attended minus unattended) to reduce bias from large pial and penetrating vessels[33,39,40,55].

Directing attention to the fingers led to a marked increase in superficial-layer BOLD signals within the finger ROI ($t(15) = 4.76$, $p < 0.001$, $d = 1.19$; 93.8% of participants) and a decrease in deep-layer BOLD signals ($t(15) = -3.82$, $p = 0.002$, $d = -0.95$; 75.0%) (Fig. 4c, e). In contrast, middle-layer signals did not change significantly, despite a small, non-significant reduction ($t(15) = -1.43$, $p = 0.17$, $d = -0.36$; 68.8%), suggesting that thalamic input was not modulated by attention (Fig. 4c, e). One might expect that attentional enhancement of superficial-layer responses down-regulates deep-layer activity; however, we found no relationship between attention-induced changes in the superficial and deep layers at the subject level ($R^2 = 0.04$, $p = 0.458$; Supplementary Fig. 7), likely reflecting substantial inter-subject variability.

Interestingly, attention produced a near-complete suppression—or even slightly negative signals—in the wrist ROI across all cortical layers in all participants. This suppression was greatest in the middle layer ($t(15) = -13.17$, $p < 0.001$, $d = -3.29$), followed by the deep layer ($t(15) = -11.57$, $p < 0.001$, $d = -2.89$) and the superficial layer ($t(15) = -6.13$, $p < 0.001$, $d = -1.53$) (Fig. 4d, f).

These layer-specific patterns were further supported by a two-way repeated-measures ANOVA with Condition (passive, attended) and

https://doi.org/10.1038/s41467-026-71842-w

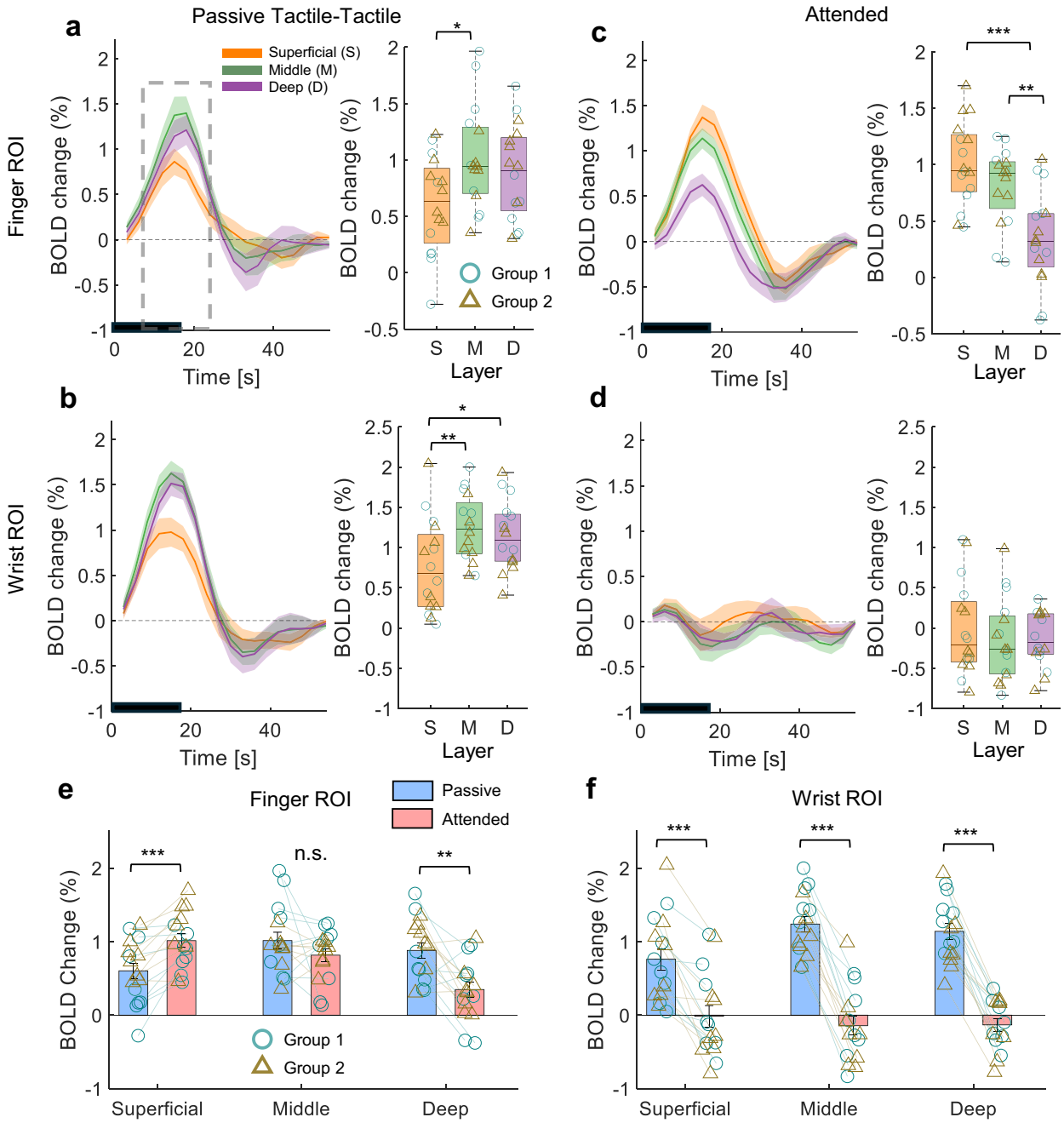

Fig. 4 | Layer-specific modulation of BOLD signals by attention in the somatosensory cortex. Time courses (left) and mean percent BOLD signal change during stimulation (18 s window, dashed box) for each cortical layer (right) in the passive condition, shown separately for the finger (**a**) and wrist (**b**) ROIs. Boxplots reflect distributions across subjects. Cyan circles represent data from Group 1, while golden triangles represent Group 2. In the finger ROI (**a**), a significant main effect of layer was observed (one-way ANOVA, $F(2,30) = 5.465$, $p = 0.009$). Post hoc Tukey's HSD tests revealed that the middle layer showed significantly stronger activation than the superficial layer (Tukey's HSD, $p = 0.021$). In the wrist ROI (**b**), both the middle and deep layers showed greater activation than the superficial layer (Tukey's HSD, $p = 0.005$ and 0.046, respectively; ANOVA, $F(2,30) = 8.503$, $p = 0.001$). Time courses and percent signal change in the attended condition for the finger (**c**) and wrist (**d**) ROIs. In the finger ROI (**c**), a significant effect of layer was again observed (ANOVA, $F(2,30) = 15.620$, $p < 0.001$). Tukey's HSD tests showed that the superficial layer exhibited greater activation than the deep layer (Tukey's HSD, $p < 0.001$), and the deep layer showed less activation than the middle layer (Tukey's HSD, $p = 0.006$). In the wrist ROI (**d**), no significant layer differences were observed (ANOVA, $F(2,30) = 0.584$, $p = 0.564$), suggesting uniform attentional suppression across layers. Asterisks in panels a–c indicate significant Tukey's HSD post hoc comparisons (multiple-comparison corrected within each ANOVA). Layer-specific BOLD modulation (passive vs attended) in the finger (**e**) and wrist (**f**) ROIs. Bars show mean percent signal change, with paired markers indicating within-subject effects. Asterisks in (**e**, **f**) denote significant passive-attended differences after Benjamini-Hochberg FDR correction across the three layers within each ROI ($q < 0.05$). In (**a**–**d**), lines represent the mean across subjects and shaded bands indicate ± SEM. Boxplots show the median (center line), interquartile range (box), and 1.5 × IQR whiskers. In (**e**, **f**), bars represent the mean ± SEM across subjects. Data are derived from $n = 16$ independent participants. All statistical tests were two-sided.

Layer (superficial, middle, deep), which revealed a significant interaction in both the finger ROI ($F(2,30) = 27.51$, $p < 0.001$, partial $\eta^2 = 0.647$) and the wrist ROI ($F(2,30) = 8.34$, $p = 0.001$, partial $\eta^2 = 0.357$), confirming that attentional modulation varied systematically with cortical depth. Also, these laminar patterns were largely consistent when we divided the data into the original eight participants and the additional eight participants (in Fig. 4, Group 1 and Group 2 are denoted by distinct symbols; see also Supplementary Fig. 6 for the results presented separately for each group).

Wrist-region activation remains suppressed, even when distracting pain stimuli are applied directly to the wrist

We next examined whether the attention-modulated, layer-specific BOLD signals observed in Experiment 1 were also present in Experiment 2, which included distracting painful stimulation. The same analyses were conducted in nine subjects (Fig. 5a–d). Attention increased superficial-layer signals and decreased deep-layer signals in the attention-driven finger ROI (Fig. 5e), while middle-layer signals in the finger ROI remained unchanged (Fig. 5e) and signals in the distracted wrist ROI were uniformly suppressed across all layers (Fig. 5f). As in Experiment 1, the cross-participant correlation between superficial-layer enhancement and deep-layer suppression was not significant ($R^2 = 0.07$, $p = 0.498$; Supplementary Fig. 7). Despite the use of a more potent distractor, the overall pattern of attentional modulation closely mirrored that observed with the tactile distractor, indicating that these laminar effects are robust and consistently reproducible across different types of distractors.

Behavioral correlates of suppressed wrist-region activity during finger-directed attention

The absence of BOLD responses across all layers of the wrist region when attention was directed to the fingers prompted a separate psychophysical experiment outside the scanner to investigate its potential behavioral consequences. Twelve participants were instructed to identify the exact location of a tactile stimulus randomly applied to one of eight possible spots on the forearm (Fig. 6a). This experiment consisted of two tasks: in the first four blocks of trials, participants performed a single wrist tactile stimulation task, and in the subsequent four blocks, they completed a dual-task involving wrist tactile stimulation alongside a finger attention task. In the dual-task condition, participants simultaneously performed a frequency judgment task on tactile stimuli applied to the fingers while completing the forearm localization task, thereby simulating the passive and attention conditions described in the fMRI experiments.

Figure 6b, c show confusion matrices of the conditional probabilities of participants' responses to specific tactile stimuli. In the single wrist tactile stimulation condition, participants localized stimuli accurately, as indicated by sharp diagonal peaks (mean accuracy: 0.556 ± 0.046, chance level: 0.125). The mean conditional probability for correct diagonal responses was significantly higher than for off-diagonal responses (0.5492 ± 0.0462 vs. 0.2286 ± 0.0224; $t(11) = 5.159$, $p = 3.45 \times 10^{-4}$, Cohen's $d = 1.489$) (Fig. 6b).

In contrast, during the wrist tactile stimulation with the finger attention task, participants' responses were more dispersed, showing a bias toward locating stimuli near the center of the forearm. Mean accuracy in this dual-task condition was significantly lower (0.1232 ± 0.0112) than the single wrist tactile stimulation condition (mean difference: 0.4324 ± 0.0419; $t(11) = 10.21$, $p = 6.03 \times 10^{-7}$, Cohen's $d = 2.95$), with the chance level at 0.125. The mean values of conditional probability for diagonal versus off-diagonal responses were 0.1235 ± 0.0113 and 0.1477 ± 0.0028, respectively ($t(11) = -1.853$, $p = 0.091$, Cohen's $d = -0.535$) (Fig. 6c). The similar probabilities between correct and incorrect perception suggest that attentional resources were almost entirely allocated to the finger task, leaving insufficient capacity to process task-irrelevant input.

These results suggest that diverting attention away from the forearm to the fingers impairs sensory discrimination, consistent with the absence of BOLD responses in the unattended wrist region when attention is directed to the fingers.

Discussion

We utilized spin-echo BOLD imaging at ultra-high field strength to investigate how layer-specific computations in S1 support selective attention. We found that (1) attention selectively enhanced activity in the superficial layer while suppressing deep-layer responses, and (2) attention broadly suppressed activity across all layers in distractor regions, even when the distractor was a noxious stimulus. Furthermore, an additional behavioral experiment revealed that distraction impaired sensory discrimination, consistent with the absence of significant BOLD activation in the unattended wrist region.

Our study represents an advance in laminar fMRI methodology. Traditionally, layer-specific analyses with gradient-echo BOLD (GE-BOLD) data rely on subtraction methods to isolate task effects[33,39,40,55,56]. For example, researchers often subtract activation maps from two task conditions (e.g., attended minus unattended, or stimulation minus baseline) to remove common large-vessel contributions and emphasize condition-specific differences. While effective for highlighting contrasts, such subtraction approaches can obscure nonlinear response patterns or baseline variability caused by large-vessel bias, because the superficial layer lies closest to the pial surface where large draining veins are located, and the influence of these vessels does not vary linearly across layers[57,58]. By using SE-BOLD —which minimizes large-vessel bias and emphasizes microvascular changes—we directly measured laminar activation without relying on subtraction, enabling a more precise characterization of layer-specific responses[42,46,59]. Although laminar-resolution SE-BOLD fMRI offers greater specificity than GE-BOLD fMRI, this advantage comes with reduced sensitivity. Thus, achieving robust microvascular signals requires ultra-high magnetic field strengths (e.g., 7 T) and extensive signal averaging across a large number of repeated trials.

With this methodological advantage, our results reveal how attention modulates neural responses in the sensory cortex. Elevated superficial-layer activity during attention likely reflects enhanced encoding of behaviorally relevant input, consistent with prior laminar fMRI findings[38,39,60]. In contrast, we observed suppression in the deep layer. In nonhuman primates, attention reduces alpha-band modulation in deep layers[34]. Although direct comparison between BOLD responses and neurophysiological alpha-band modulation is challenging, both measures reflect local neuronal activity, providing converging evidence for layer-specific attentional effects. Interestingly, some laminar fMRI studies in humans report increased deep-layer responses for illusory or predicted stimuli—specifically, in primary visual cortex (V1) for illusory contours[40] and in S1 for predicted tactile inputs during sequential tapping[55]. While attention to a present stimulus differs from anticipating a feature in its absence, these seemingly opposite modulations—suppression during attention versus enhancement during prediction—can be reconciled within a predictive coding framework: attention suppresses irrelevant outputs to sharpen selection, whereas prediction enhances feedback to minimize error, with deep-layer feedback conveying internal models to lower-level sensory areas[61,62]. Direct comparisons between these conditions remain an important direction for future work.

An important finding was the marked suppression of S1 responses to unattended wrist distractors. This suppression occurred across all layers and persisted throughout stimulation, suggesting that attention can filter irrelevant input by modulating early sensory pathways, possibly via thalamic gating[63–67]. Such gating could reflect a broad inhibitory control signal[68–70], supported by evidence that attentional modulation of the thalamus can induce widespread cortical inhibition[66,71,72]. Alternatively, the normalization model of attention[73]

https://doi.org/10.1038/s41467-026-71842-w

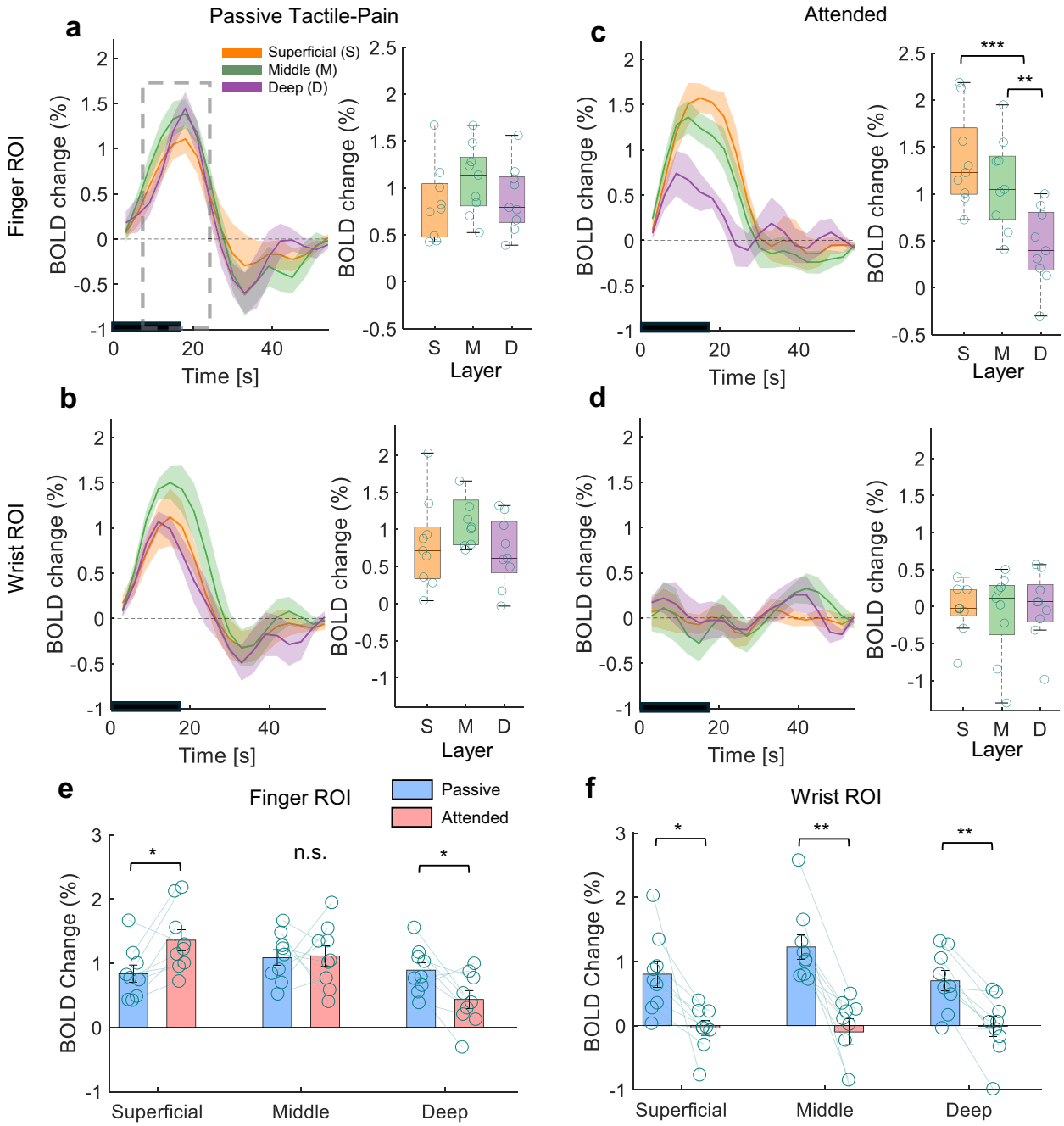

Fig. 5 | Layer-specific modulation of BOLD signals by attention in the somatosensory cortex in Experiment 2. Time courses (left) and mean percent BOLD signal change during stimulation (right) for each layer in the passive condition, shown separately for the finger (**a**) and wrist (**b**) ROIs. Lines represent the mean across subjects and shaded bands indicate ± SEM. Boxplots reflect subject-level distributions. In the finger ROI (**a**) and wrist ROI (**b**), the middle layer showed numerically higher responses, though the layer effect was not significant ($F(2,16) = 1.847$, $p = 0.190$; $F(2,16) = 2.859$, $p = 0.087$, respectively). Same plots for the attended condition. In the finger ROI (**c**), a significant effect of layer was observed ($F(2,16) = 10.049$, $p = 0.001$). Tukey's HSD tests showed greater activation in the superficial vs. deep layer (Tukey's HSD, $p < 0.001$) and less activation in the deep vs. middle layer (Tukey's HSD, $p = 0.008$). In the wrist ROI (**d**), no significant effect of layer was found ($F(2,16) = 0.202$, $p = 0.819$). Asterisks in panel c indicate significant Tukey's HSD post hoc comparisons (multiple-comparison corrected within each ANOVA). Attention-related BOLD modulation (passive vs. attended) in the finger (**e**) and wrist (**f**) ROIs. Bars show mean; paired dots reflect within-subject differences. A significant Condition × Layer interaction was found only in the finger ROI ($F(2,16) = 9.804$, $p = 0.002$, $\eta^2 = 0.551$); the wrist ROI showed a main effect of condition ($F(1,8) = 38.218$, $p < 0.001$, $\eta^2 = 0.827$) but no interaction ($F(2,16) = 2.288$, $p = 0.134$). Paired t-tests in the finger ROI revealed increased signals in the superficial layer ($t(8) = 3.034$, $p = 0.016$, $d = 1.011$), no significant change in the middle layer ($p = 0.906$), and suppression in the deep layer ($t(8) = -2.793$, $p = 0.023$, $d = -0.931$). In the wrist ROI, all layers were significantly suppressed (all $p < 0.015$). Asterisks in (**e**, **f**) denote significant passive-attended differences after Benjamini-Hochberg FDR correction across the three layers within each ROI ($q < 0.05$). In (**a**–**d**), lines represent the mean across subjects and shaded bands indicate ± SEM. Boxplots show the median (center line), interquartile range (box), and 1.5 × IQR whiskers. In (**e**, **f**), bars represent the mean ± SEM across subjects. Data are derived from $n = 9$ independent participants. All statistical tests were two-sided.

https://doi.org/10.1038/s41467-026-71842-w

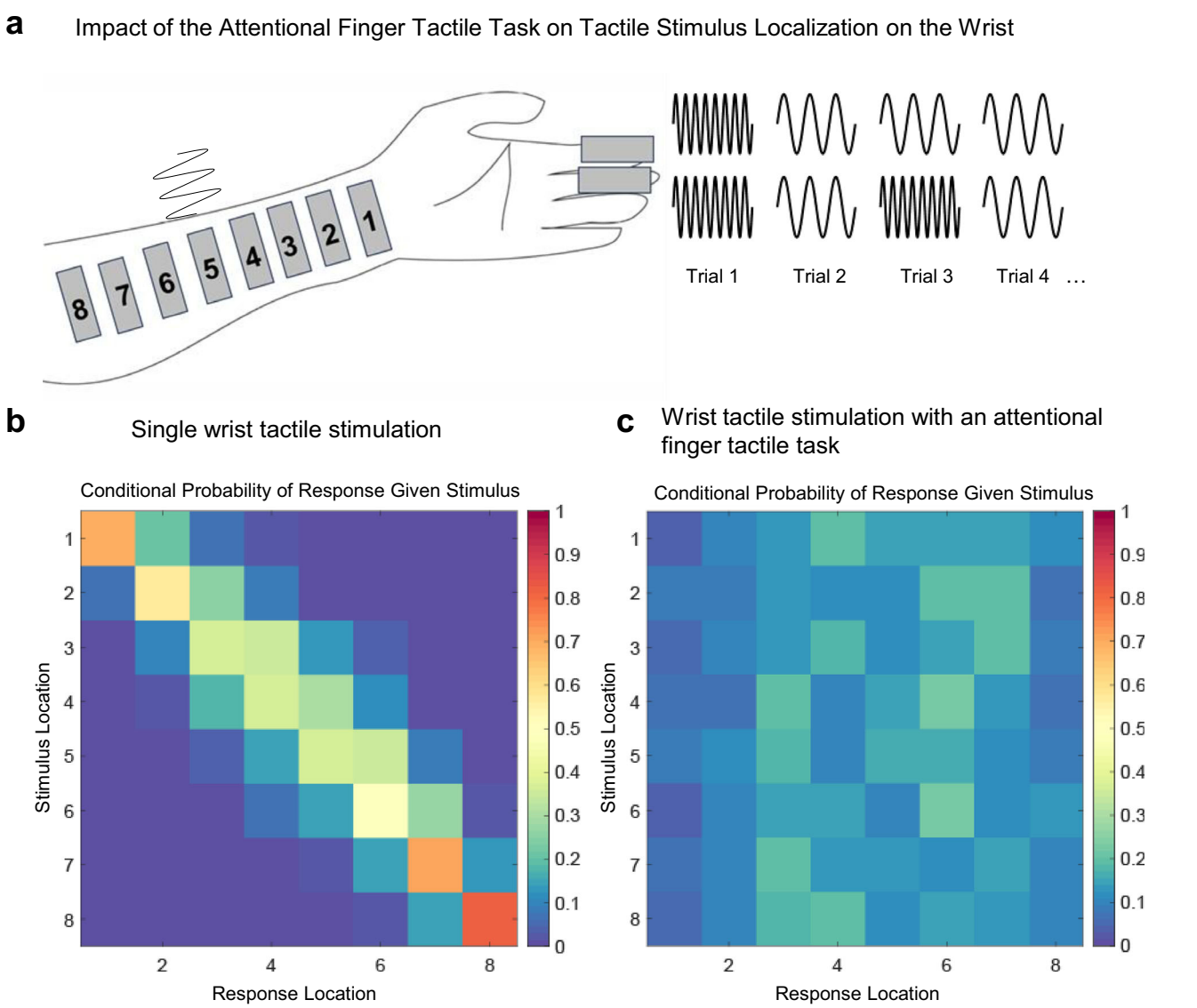

Fig. 6 | Impact of the Attentional Finger Tactile Task on Tactile Stimulus Location Identification on the Wrist. a Participants ($n = 12$) underwent eight blocks of 32 trials each. During the first four blocks (single wrist tactile stimulation), they were instructed to locate a tactile stimulus randomly applied to one of eight positions on the forearm. In the subsequent four blocks (wrist tactile stimulation with a finger attention task), participants performed a dual task: they first judged whether tactile stimuli on the fingers differed in frequency and then identified the stimulus location on the forearm. **b** The conditional probability matrix (i.e., confusion matrix) for the single wrist tactile stimulation condition. The x-axis indicates response locations, and the y-axis represents true stimulus locations on the forearm. Clear diagonal peaks suggest a strong correspondence between stimulus and response locations, indicating high identification accuracy. **c** The conditional probability matrix for the wrist tactile stimulation with the finger attention task. The response distribution is more dispersed, with reduced diagonal peaks, indicating impaired accuracy in identifying forearm stimulus locations when attention is divided. This finding supports the conclusion that attentional focus on finger stimuli compromises the processing of forearm stimuli.

describes attentional effects as emerging from a divisive balance between excitatory drive and suppressive surround activity. Under conditions where suppressive drive dominates, normalization can lead to overall reductions in response amplitude, which may contribute to the broad suppression observed in the unattended wrist representation.

In contrast, the attended finger representation exhibited uneven, layer-dependent modulations—strong enhancement in superficial layers, minimal change in the thalamic-input middle layers, and reduced responses in deep layers. This laminar pattern aligns more closely with a cortical gating mechanism, although normalization and gating are not mutually exclusive and may jointly operate depending on stimulus and task demands. A gating mechanism is also consistent with our behavioral data and prior evidence that attentional modulation of the thalamus can induce widespread cortical inhibition[66,71,72].

However, testing the thalamic gating hypothesis directly was beyond the scope of this study, as our high-resolution SE-BOLD protocol required limited spatial coverage. Specifically, SE-BOLD fMRI is constrained by the number of slices that can be acquired due to specific absorption rate (SAR) limits and the need for adequate temporal resolution. Consequently, we acquired only an oblique slab covering the contralateral sensorimotor regions, precluding whole-brain imaging, including attention-modulated areas such as the prefrontal cortex and thalamus. Future high-resolution fMRI studies that explicitly target the thalamus during the same passive and attention-demanding tasks will be crucial for directly testing the gating mechanism.

Despite several advancements we have made, there are many potential limitations to our study. First, although both stimulus conditions produced similar results in the finger and wrist regions, attention was directed only to the fingers, not to the wrist. To

determine whether our findings generalize to other attended regions, it is essential to conduct experiments involving attention directed to the wrist. Second, our spatial resolution imposes inherent limitations. We used a 0.8 mm isotropic voxel size—typical for layer-specific fMRI[33,40,42,46]—but insufficient to cleanly separate signals from the three cortical layers, given the ~2 mm thickness of human S1. As shown in Fig. 2d (right), our middle-layer ROI spans both layer 4 (true middle) and layer 5. Because layer 4 is thinner than a single 0.8 mm voxel, partial volume effects likely introduced layer 5 contributions into the "middle"-layer signals. Moreover, the point spread function (PSF) further blurs signals across layers[56,74–78], and variability in neurovascular coupling adds additional complexity[74,75,79,80]. Achieving higher spatial resolution with advanced imaging technologies will be critical for more precise layer-specific mapping in humans. Third, the finger and wrist ROIs were defined using phase-sensitive traveling-wave tactile stimulation and further refined based on actual task data. Therefore, the ROIs are not entirely independent, raising the possibility of circular reasoning due to activity-dependent ROI definition. However, we believe this concern is minimal, as analyses based on anatomically defined ROIs (Fig. 3) yielded results similar to those obtained with functionally defined ROIs (Figs. 4, 5). Fourth, attention induced a small negative change in Column 3 (Fig. 3c and Supplementary Fig. 4c), whereas the wrist ROI showed near-zero but not negative BOLD responses in Figs. 4 and 5. This discrepancy likely reflects differences between the two ROI definitions: Column 3 represents a single columnar segment along the somatotopic axis, whereas the wrist ROI corresponds to a functionally defined region centered on the wrist representation derived from the localizer. Although neither the wrist ROI nor Column 3 showed significant negative BOLD after FDR correction, the visually apparent negative deflection in Column 3 is consistent with established physiological mechanisms, including local decreases in neuronal activity[81], vascular steal effects[82], and surround suppression or reduced synaptic input[56,83]. Future studies are warranted to elucidate the origin of these negative BOLD responses. Fifth, in our fMRI studies, we prioritized high spatial resolution and specificity at the expense of temporal resolution. As a result, we were unable to examine the dynamics and interaction between layers that would be informative in inferring energy efficiency of cognitive processes, which have been studied at the network level[84]. In future studies, it would be valuable to adopt high temporal resolution techniques—such as gradient-echo BOLD fMRI—to investigate the dynamics of fMRI signals across brain regions and cortical layers. Sixth, in our behavioral attention studies focused on the fingers, accuracy in discriminating among eight wrist locations was near chance, likely due to the difficulty of the task. Simpler distractor paradigms—such as a two-location wrist task—may help disentangle attention effects from task difficulty.

In summary, we demonstrate that attention elicits robust, layer-specific modulation in human S1, enhancing responses in superficial layers while suppressing deep-layer output in the attended region. At the same time, attention induces widespread suppression in regions processing irrelevant inputs. Together, these processes may be critical for efficient perceptual processing and precise attentional control.

Methods

Participants and MRI system

Seventeen healthy participants (ten males and seven females), aged 25–49 years (mean age: 34 years, standard deviation: 8.01 years), participated across Experiments 1 ($n = 16$) and 2 ($n = 9$) of our fMRI study. Additionally, twelve participants (eight males and four females), aged 19–25 years (mean age: 23 years, standard deviation: 1.65 years), took part in the behavioral experiment. Sex was self-reported by participants. No sex-based analyses were performed because the study was not powered to detect sex differences. All experiments were approved by the Institutional Review Board of Sungkyunkwan University and conducted in accordance with the Declaration of Helsinki. All subjects were thoroughly informed about the procedures and provided written consent prior to participation.

Task paradigms

A tactile discrimination task was employed to direct participants' attention to tactile stimuli on their fingers while additional tactile or thermal stimuli were simultaneously presented on their wrists as unattended (Fig. 1c–f). Each stimulus lasted 18 s (Fig. 1f), aiming to examine neural response differences during active task engagement compared to passive conditions. To ensure that the task and passive conditions were matched in motor demands, no behavioral responses were required during stimulus presentation.

Experiment 1 involved sixteen participants who received tactile stimuli on their left index and middle fingers and on their left wrist, as depicted in Fig. 1c. Four MR-compatible PTS Piezo Tactile Stimulator stimulators (Dancer design, UK) were used to deliver tactile stimuli at frequencies of either 3 Hz or 8 Hz. The frequencies were randomized across trials to ensure varied sensory input, as detailed in Fig. 1d. This setup allowed us to investigate how directed attention towards stimuli on the fingers could influence the processing of concurrent, unattended distractor stimuli on the wrist.

Experiment 2 introduced a thermal stimulus at the wrist as an additional unattended variable while continuing the tactile discrimination task on the fingers for nine participants, including eight from Experiment 1 and one new participant, as illustrated in Fig. 1e. The thermal stimulus, set at 44 degrees Celsius to activate nociceptors, was perceptibly noticeable and sufficiently distracting, as described in Fig. 1e. In this setup, an MR-compatible thermode (CHEPS, Pathway system, Medoc, Israel) was attached to the wrist and used to deliver thermal stimulation. The temperature ramped up from a baseline of 32 °C to 44 °C over 5.5 s, remained at a plateau of 44 °C for 7 s, and then ramped back down to baseline over another 5.5 s (Fig.1f). Each stimulus presentation lasted 18 s, followed by a 36-s rest period, repeated eight times per run, alternating between task and passive conditions across eight total runs.

For the behavioral experiment, twelve additional participants engaged in eight blocks, each consisting of 32 trials. The first four blocks involved a single wrist tactile stimulation condition where participants identified the precise location of a tactile stimulus randomly presented at one of eight locations on the forearm (Fig. 6a). The subsequent four blocks were wrist tactile stimulation with an attentional finger tactile task, where participants first assessed whether the frequencies of tactile stimuli on their fingers were the same or different, followed by identifying the specific location of the stimulus on their forearm.

Layer-specific fMRI data acquisition

The measurements were conducted on a 7 T scanner (MAGNETOM Terra, Siemens Healthineers, Erlangen, Germany) equipped with a single-channel transmitter and a 32-channel receive head coil (NOVA Medical, Wilmington, MA). To minimize subject movement, MR-compatible cushions securely padded the space inside the coil. Anatomical images were obtained using the MP2RAGE sequence[85] with the following imaging parameters: sagittal orientation, 0.7 mm isotropic resolution, field of view (FOV) of $224 \times 210 \times 168$ mm^3, R inplane = 3, inversion times (TIs) of 1.0/3.2 s, TE of 2.29 ms, TR of 4500 ms, readout bandwidth of 200 Hz/Px, and flip angle of 4°.

To obtain layer-dependent fMRI responses, oblique slices were targeted to regions of the human primary sensory cortex (S1) adjacent to the central sulcus. We employed a multi-shot segmented spin and gradient echo (SAGE) EPI approach to achieve high spatial resolution fMRI and overcome the spatial encoding limitations of single-shot EPI[42,46]. The multi-shot SAGE EPI imaging parameters included a 0.8×0.8 mm^2 in-plane resolution, Rin-plane = 9 (for each shot; effective Rin-plane = 3 by 3 shots), FOV of 144×144 mm^2,

37 slices (slice thickness of 0.8 mm), a flip angle pair of 90–180°, partial Fourier of 6/8, echo spacing (ESP) of 1 ms (1282 Hz/Px), and a TR for each shot of 3000 ms. TE GE/TE SE were 14/56.84 ms. The EPI readout per shot was 12 ms, which is near the optimal values for a readout window of around $0.5 \times T_2^*$ to minimize T_2^* contamination[42,46]. For distortion correction of EPI images, a B_0 field map was acquired using FLASH images with the same imaging parameters as the SAGE EPI, except for a bandwidth of 620 Hz/Px, TEs of 3.3, 6.3 ms, and a flip angle of 50°.

An 8-minute task paradigm involved alternating blocks of 18 s of tactile stimulation and 36 s of rest, starting with an initial 36-s rest period. Slices were precisely positioned perpendicular to the central sulcus between the motor and sensory cortices (M1 and S1)[42–45].

Somatotopic mapping and ROI localization

To identify somatotopic representations of fingers and wrist within primary somatosensory cortex (S1), we employed a phase-encoded tactile traveling wave (TW) paradigm (Supplementary Fig. 1a)[51]. Four body sites—fingers, hand, wrist, and forearm—were stimulated sequentially every 10 s in forward (0° to 270°) or reverse (270° to 0°) order. Each participant underwent six runs.

Localizer scans were acquired in an independent scanning session using a gradient-echo EPI sequence (0.8 mm isotropic resolution, TR = 2 s, TE = 20 ms, 25 slices from 15 out of 17 participants, including all participants except one in Experiment 1 (Group 1: $n = 7$, Group 2: $n = 8$). In Experiment 2, no new localizer runs were conducted, as participants P1–P7 had already completed the localizer in Experiment 1. The only participant who took part exclusively in Experiment 2 did not undergo the localizer.

Phase values were computed using Fourier analysis, and circular means revealed location-specific preferences (Supplementary Fig. 1b). Voxels with an $r > 0.06$ were selected to visualize reliable tuning (Fig. 2a), revealing a somatotopic progression along the posterior bank of the central sulcus (area 3b). ROIs were defined from finger- and wrist-preferring voxels. For the two participants without localizer data, ROIs were identified from the main task activation maps using anatomical landmarks, such as the hand knob, and functional overlap between passive and task conditions (Fig. 2b and Supplementary Fig. 2).

Layer-specific fMRI data preprocessing and functional analysis

K-space data were reconstructed using a sliding-window concept to maintain temporal resolution with specific shot repetition times[42], utilizing a custom MATLAB script (MathWorks, Natick, MA). For example, three shots—TRshot (2), TRshot (3), and TRshot (4)—were combined for image reconstruction, enhancing the clarity and quality of the images. Nyquist ghost correction and phase offset correction were performed independently for each shot. The combined data then underwent conventional Generalized Autocalibrating Partial Parallel Acquisition (GRAPPA).

The preprocessing pipeline was adopted from the previous studies[42,46]. Functional runs were first concatenated and then underwent motion correction using SPM12 (Functional Imaging Laboratory, University College London, UK) with six motion parameters. To improve signal-to-noise ratio for laminar analysis, all repeated runs were motion-corrected and averaged without additional spatial alignment, preserving the native functional space for subsequent analyses. The fMRI data were then upsampled to a fourfold finer in-plane grid ($0.2 \times 0.2\ mm^2$) using cubic interpolation to facilitate alignment with cortical-depth estimates[42,46]. Distortions in the EPI images were corrected using a B_0 field map processed with PRELUDE and FUGUE from FSL package, ensuring alignment with scanner-specific echo spacing and unwarping parameters. Anatomical MP2RAGE images were co-registered to the motion- and distortion-corrected functional images using SPM12.

A mask of the 3b region of the primary sensory cortex (S1) was generated using FreeSurfer. Cerebrospinal fluid (CSF), gray matter, and white matter were visually identified from the anatomical images, aiding in the creation of precise layer masks for subsequent analysis. All data analyses were conducted using custom-written MATLAB scripts. For statistical analyses, spatial smoothing with a Gaussian kernel of 1.6 mm (twice the voxel size of $0.8\ mm^3$) was applied using FSL FEAT[86] to facilitate the manual drawing of regions of interest (ROIs) from the activation maps. However, for layer-specific and columnar analyses, all steps were performed without spatial smoothing to preserve the native resolution of the data, ensuring precise measurements of layer-specific and columnar activity (see the section below, *Region of Interest (ROI) Selection and Columnar Analysis*, for details).

Functional activation mapping and percent signal change

Functional activation maps were created by averaging BOLD signals across individual trials for each condition (task and passive), followed by a General Linear Model (GLM) analysis using a canonical hemodynamic response function (HRF) to produce *z*-statistic maps. A primary threshold of $z > 1.5$ was applied, and results were cluster-corrected at $p < 0.05$. Passive activation maps generally included both wrist and finger responses, while task maps primarily highlighted finger representations.

Percent signal change was computed by subtracting the mean BOLD signal during the 6 s prior to stimulus onset (baseline) from the signal during stimulation, dividing by the baseline, and multiplying by 100. The stimulation duration was 18 s (6 TRs; TR = 3 s), and BOLD responses were averaged over the full 18-s window, starting 2 TRs (6 s) after stimulus onset to account for the hemodynamic delay.

Columnar analyses

To examine fine-scale spatial patterns, columnar ROIs were manually defined along the somatotopic axis of area 3b, covering transitions from wrist to finger representations (Fig. 3a and Supplementary Fig. 4a). These ROIs were divided into five columnar segments, each representing a contiguous band of cortex. For each condition, signal time courses were extracted across columns. This allowed for visualization of attentional modulation across somatotopic space. Average signal change during stimulation was compared across columns, and columns 1–5 were tested for condition × location interaction effects.

Laminar profile and layer assignment

Finger and wrist ROIs were manually drawn on GE/SE BOLD ratio images, which provided high contrast between tissue types and enabled clear visualization of both the CSF–GM boundary and the GM–WM boundary (Fig. 2c). ROIs were centered on finger- and wrist-preferring voxels identified from an independent somatotopic localizer (or task activation maps in the absence of a localizer; see *Somatotopic Mapping and ROI Localization*). These delineations allowed precise identification of the full cortical ribbon in area 3b of S1 for laminar analysis. Following this delineation, cortical depth bins were generated using the LAYNII software suite[87], which divides the ribbon into 8 equivolume bins, spanning the ~2 mm cortical thickness of S1[45] (Fig. 2c). To reduce slice-selection bias and improve statistical power, laminar profiles were averaged across slices within the manually defined ROIs. Percent signal changes were then calculated for each bin.

To validate the laminar structure, quantitative T_1 (qT_1) maps from MP2RAGE data were analyzed (Fig. 2d and Supplementary Fig. 3)[52]. qT_1 values decreased monotonically from the pial surface to the WM boundary. First and second derivatives revealed consistent transitions and inflection points across subjects (Supplementary Fig. 3b–d),

supporting known laminar boundaries. Based on the qT_1 gradient analysis and relative cortical depth, we grouped cortical depth bins into three laminar compartments: Bins 1–2 were designated as superficial layers, Bins 4–5 as middle layers, and Bins 7–8 as deep layers.

Statistical analysis

Unless otherwise specified, statistical analyses in the main text report uncorrected *p* values. For multiple comparisons across ROIs or cortical layers, we applied the Benjamini-Hochberg false-discovery-rate (FDR) procedure ($q < 0.05$). Specifically, one-sample and paired *t*-tests across the five columnar ROIs and across the three cortical layers were corrected within each family of tests. Statistical significance in the figures is indicated using FDR-corrected thresholds.

Reporting summary

Further information on research design is available in the Nature Portfolio Reporting Summary linked to this article.

Data availability

All data supporting the findings of this study are available on the Open Science Framework (OSF) at https://osf.io/2v6nb/. Source data are provided with this paper.

Code availability

Custom MATLAB scripts used for the analysis of laminar spin-echo fMRI data are available at: https://github.com/dhkim15/S1-laminar-attention-SEBOLD (Release v1.0).

References

1. Posner, M. I. & Petersen, S. E. The attention system of the human brain. *Annu. Rev. Neurosci.* **13**, 25–42 (1990).
2. Desimone, R. & Duncan, J. Neural mechanisms of selective visual attention. *Annu. Rev. Neurosci.* **18**, 193–222 (1995).
3. Luck, S. J., Chelazzi, L., Hillyard, S. A. & Desimone, R. Neural mechanisms of spatial selective attention in areas V1, V2, and V4 of macaque visual cortex. *J. Neurophysiol.* **77**, 24–42 (1997).
4. Reynolds, J. H. & Chelazzi, L. Attentional modulation of visual processing. *Annu. Rev. Neurosci.* **27**, 611–647 (2004).
5. Kastner, S., De Weerd, P., Desimone, R. & Ungerleider, L. G. Mechanisms of directed attention in the human extrastriate cortex as revealed by functional MRI. *Science* **282**, 108–111 (1998).
6. McAdams, C. J. & Maunsell, J. H. Effects of attention on orientation-tuning functions of single neurons in macaque cortical area V4. *J. Neurosci.* **19**, 431–441 (1999).
7. Reynolds, J. H., Chelazzi, L. & Desimone, R. Competitive mechanisms subserve attention in macaque areas V2 and V4. *J. Neurosci.* **19**, 1736–1753 (1999).
8. Kastner, S. & Ungerleider, L. G. Mechanisms of visual attention in the human cortex. *Annu. Rev. Neurosci.* **23**, 315–341 (2000).
9. Williford, T. & Maunsell, J. H. Effects of spatial attention on contrast response functions in macaque area V4. *J. Neurophysiol.* **96**, 40–54 (2006).
10. Mountcastle, V. B. Modality and topographic properties of single neurons of cat's somatic sensory cortex. *J. Neurophysiol.* **20**, 408–434 (1957).
11. Kandel, E. R. et al. *Principles of neural science*, 4th edn (McGraw-hill New York, 2000).
12. Hubel, D. H. & Wiesel, T. N. Receptive fields and functional architecture of monkey striate cortex. *J. Physiol.* **195**, 215–243 (1968).
13. Van Essen, D. C., Newsome, W. T. & Maunsell, J. H. The visual field representation in striate cortex of the macaque monkey: asymmetries, anisotropies, and individual variability. *Vis. Res.* **24**, 429–448 (1984).
14. Somers, D. C., Dale, A. M., Seiffert, A. E. & Tootell, R. B. Functional MRI reveals spatially specific attentional modulation in human primary visual cortex. *Proc. Natl. Acad. Sci. USA* **96**, 1663–1668 (1999).
15. Gandhi, S. P., Heeger, D. J. & Boynton, G. M. Spatial attention affects brain activity in human primary visual cortex. *Proc. Natl. Acad. Sci. USA* **96**, 3314–3319 (1999).
16. Tootell, R. B. et al. The retinotopy of visual spatial attention. *Neuron* **21**, 1409–1422 (1998).
17. McAdams, C. J. & Reid, R. C. Attention modulates the responses of simple cells in monkey primary visual cortex. *J. Neurosci.* **25**, 11023–11033 (2005).
18. Gomez-Ramirez, M., Hysaj, K. & Niebur, E. Neural mechanisms of selective attention in the somatosensory system. *J. Neurophysiol.* **116**, 1218–1231 (2016).
19. Hsiao, S. S., O'Shaughnessy, D. M. & Johnson, K. O. Effects of selective attention on spatial form processing in monkey primary and secondary somatosensory cortex. *J. Neurophysiol.* **70**, 444–447 (1993).
20. Steinmetz, P. N. et al. Attention modulates synchronized neuronal firing in primate somatosensory cortex. *Nature* **404**, 187–190 (2000).
21. Moran, J. & Desimone, R. Selective attention gates visual processing in the extrastriate cortex. *Science* **229**, 782–784 (1985).
22. Buschman, T. J. & Miller, E. K. Top-down versus bottom-up control of attention in the prefrontal and posterior parietal cortices. *Science* **315**, 1860–1862 (2007).
23. Gregoriou, G. G., Gotts, S. J., Zhou, H. & Desimone, R. High-frequency, long-range coupling between prefrontal and visual cortex during attention. *Science* **324**, 1207–1210 (2009).
24. Molyneaux, B. J., Arlotta, P., Menezes, J. R. & Macklis, J. D. Neuronal subtype specification in the cerebral cortex. *Nat. Rev. Neurosci.* **8**, 427–437 (2007).
25. Kaas, J. H. The evolution of the complex sensory and motor systems of the human brain. *Brain Res. Bull.* **75**, 384–390 (2008).
26. Thomson, A. M. & Lamy, C. Functional maps of neocortical local circuitry. *Front. Neurosci.* **1**, 19–42 (2007).
27. Constantinople, C. M. & Bruno, R. M. Deep cortical layers are activated directly by thalamus. *Science* **340**, 1591–1594 (2013).
28. Palomero-Gallagher, N. & Zilles, K. Cortical layers: Cyto-, myelo-, receptor- and synaptic architecture in human cortical areas. *Neuroimage* **197**, 716–741 (2019).
29. Liao, C. C., Gharbawie, O. A., Qi, H. & Kaas, J. H. Cortical connections to single digit representations in area 3b of somatosensory cortex in squirrel monkeys and prosimian galagos. *J. Comp. Neurol.* **521**, 3768–3790 (2013).
30. Thomson, A. M. & Bannister, A. P. Interlaminar connections in the neocortex. *Cereb. Cortex* **13**, 5–14 (2003).
31. Liang, M., Mouraux, A., Hu, L. & Iannetti, G. D. Primary sensory cortices contain distinguishable spatial patterns of activity for each sense. *Nat. Commun.* **4**, 1979 (2013).
32. Nandy, A. S., Nassi, J. J. & Reynolds, J. H. Laminar organization of attentional modulation in macaque visual area V4. *Neuron* **93**, 235–246 (2017).
33. Lawrence, S. J., Norris, D. G. & de Lange, F. P. Dissociable laminar profiles of concurrent bottom-up and top-down modulation in the human visual cortex. *Elife* **8**, e44422 (2019).
34. Buffalo, E. A., Fries, P., Landman, R., Buschman, T. J. & Desimone, R. Laminar differences in gamma and alpha coherence in the ventral stream. *Proc. Natl. Acad. Sci. USA* **108**, 11262–11267 (2011).
35. Hopf, J. M. et al. Direct neurophysiological evidence for spatial suppression surrounding the focus of attention in vision. *Proc. Natl. Acad. Sci. USA* **103**, 1053–1058 (2006).
36. Muller, M. M., Malinowski, P., Gruber, T. & Hillyard, S. A. Sustained division of the attentional spotlight. *Nature* **424**, 309–312 (2003).

37. O'Connell, M. N., Barczak, A., Schroeder, C. E. & Lakatos, P. Layer specific sharpening of frequency tuning by selective attention in primary auditory cortex. *J. Neurosci.* **34**, 16496–16508 (2014).
38. Liu, C. et al. Layer-dependent multiplicative effects of spatial attention on contrast responses in human early visual cortex. *Prog. Neurobiol.* **207**, 101897 (2021).
39. Muckli, L. et al. Contextual feedback to superficial layers of V1. *Curr. Biol.* **25**, 2690–2695 (2015).
40. Kok, P., Bains, L. J., van Mourik, T., Norris, D. G. & de Lange, F. P. Selective activation of the deep layers of the human primary visual cortex by top-down feedback. *Curr. Biol.* **26**, 371–376 (2016).
41. Demirayak, P., Deshpande, G. & Visscher, K. Laminar functional magnetic resonance imaging in vision research. *Front Neurosci.* **16**, 910443 (2022).
42. Han, S., Eun, S., Cho, H., Uludag, K. & Kim, S. G. Improvement of sensitivity and specificity for laminar BOLD fMRI with double spin-echo EPI in humans at 7 T. *Neuroimage* **241**, 118435 (2021).
43. Huber, L. et al. Sub-millimeter fMRI reveals multiple topographical digit representations that form action maps in human motor cortex. *Neuroimage* **208**, 116463 (2020).
44. Huber, L. et al. High-resolution CBV-fMRI allows mapping of laminar activity and connectivity of cortical input and output in human M1. *Neuron* **96**, 1253–1263 e1257 (2017).
45. Huber, L. et al. Cortical lamina-dependent blood volume changes in human brain at 7 T. *Neuroimage* **107**, 23–33 (2015).
46. Han, S., Eun, S., Cho, H., Uludag, K. & Kim, S. G. Improved laminar specificity and sensitivity by combining SE and GE BOLD signals. *Neuroimage* **264**, 119675 (2022).
47. Han, S., Kim, D., Eun, S., Cho, H. & Kim, S. G. 7T Spin-echo BOLD fMRI enhances spatial specificity in the human motor cortex during finger movement tasks. *Neuroimage* **317**, 121351 (2025).
48. Abraira, V. E. & Ginty, D. D. The sensory neurons of touch. *Neuron* **79**, 618–639 (2013).
49. Caterina, M. J. et al. The capsaicin receptor: a heat-activated ion channel in the pain pathway. *Nature* **389**, 816–824 (1997).
50. Kim, D., Woo, C. W. & Kim, S. G. Neural mechanisms of pain relief through paying attention to painful stimuli. *Pain* **163**, 1130–1138 (2022).
51. O'Neill, G. C. et al. A probabilistic atlas of finger dominance in the primary somatosensory cortex. *Neuroimage* **217**, 116880 (2020).
52. Doehler, J. et al. The 3D structural architecture of the human hand area is nontopographic. *J. Neurosci.* **43**, 3456–3476 (2023).
53. Dinse, J. et al. A cytoarchitecture-driven myelin model reveals area-specific signatures in human primary and secondary areas using ultra-high resolution in-vivo brain MRI. *Neuroimage* **114**, 71–87 (2015).
54. Kuehn, E. et al. Body topography parcellates human sensory and motor cortex. *Cereb. Cortex* **27**, 3790–3805 (2017).
55. Yu, Y. et al. Layer-specific activation of sensory input and predictive feedback in the human primary somatosensory cortex. *Sci. Adv.* **5**, eaav9053 (2019).
56. Logothetis, N. K., Pauls, J., Augath, M., Trinath, T. & Oeltermann, A. Neurophysiological investigation of the basis of the fMRI signal. *Nature* **412**, 150–157 (2001).
57. Koopmans, P. J., Barth, M. & Norris, D. G. Layer-specific BOLD activation in human V1. *Hum. Brain Mapp.* **31**, 1297–1304 (2010).
58. Polimeni, J. R., Fischl, B., Greve, D. N. & Wald, L. L. Laminar analysis of 7T BOLD using an imposed spatial activation pattern in human V1. *Neuroimage* **52**, 1334–1346 (2010).
59. Kim, S. G. & Ugurbil, K. High-resolution functional magnetic resonance imaging of the animal brain. *Methods* **30**, 28–41 (2003).
60. Lawrence, S. J., Formisano, E., Muckli, L. & de Lange, F. P. Laminar fMRI: applications for cognitive neuroscience. *Neuroimage* **197**, 785–791 (2019).
61. Bastos, A. M. et al. Canonical microcircuits for predictive coding. *Neuron* **76**, 695–711 (2012).
62. Friston, K. A theory of cortical responses. *Philos. Trans. R. Soc. Lond. B Biol. Sci.* **360**, 815–836 (2005).
63. Sherman, S. M. Thalamic relays and cortical functioning. *Prog. Brain Res* **149**, 107–126 (2005).
64. Sherman, S. M. & Guillery, R. W. Distinct functions for direct and transthalamic corticocortical connections. *J. Neurophysiol.* **106**, 1068–1077 (2011).
65. Sherman, S. M., Guillery, R. W. & Sherman, S. M. *Exploring the Thalamus and its Role in Cortical Function*. 2nd edn (MIT Press, 2006).
66. Crabtree, J. W. Intrathalamic sensory connections mediated by the thalamic reticular nucleus. *Cell Mol. Life Sci.* **56**, 683–700 (1999).
67. Destexhe, A., Contreras, D. & Steriade, M. Mechanisms underlying the synchronizing action of corticothalamic feedback through inhibition of thalamic relay cells. *J. Neurophysiol.* **79**, 999–1016 (1998).
68. Harris, K. D. & Shepherd, G. M. The neocortical circuit: themes and variations. *Nat. Neurosci.* **18**, 170–181 (2015).
69. Isaacson, J. S. & Scanziani, M. How inhibition shapes cortical activity. *Neuron* **72**, 231–243 (2011).
70. Tremblay, R., Lee, S. & Rudy, B. GABAergic interneurons in the neocortex: from cellular properties to circuits. *Neuron* **91**, 260–292 (2016).
71. Sherman, S. M. & Guillery, R. W. *Functional Connections of Cortical Areas: a New View from the Thalamus* (The MIT Press, 2013).
72. Harris, K. D. & Thiele, A. Cortical state and attention. *Nat. Rev. Neurosci.* **12**, 509–523 (2011).
73. Reynolds, J. H. & Heeger, D. J. The normalization model of attention. *Neuron* **61**, 168–185 (2009).
74. Kim, S. G. & Ogawa, S. Biophysical and physiological origins of blood oxygenation level-dependent fMRI signals. *J. Cereb. Blood Flow. Metab.* **32**, 1188–1206 (2012).
75. Logothetis, N. K. What we can do and what we cannot do with fMRI. *Nature* **453**, 869–878 (2008).
76. Logothetis, N. K. & Wandell, B. A. Interpreting the BOLD signal. *Annu Rev. Physiol.* **66**, 735–769 (2004).
77. Fukuda, M., Poplawsky, A. J. & Kim, S. G. Time-dependent spatial specificity of high-resolution fMRI: insights into mesoscopic neurovascular coupling. *Philos. Trans. R. Soc. Lond. B Biol. Sci.* **376**, 20190623 (2021).
78. Poplawsky, A. J., Fukuda, M. & Kim, S. G. Foundations of layer-specific fMRI and investigations of neurophysiological activity in the laminarized neocortex and olfactory bulb of animal models. *Neuroimage* **199**, 718–729 (2019).
79. Buxton, R. B., Uludag, K., Dubowitz, D. J. & Liu, T. T. Modeling the hemodynamic response to brain activation. *Neuroimage* **23**, S220–S233 (2004). **Suppl 1**.
80. Heeger, D. J. & Ress, D. What does fMRI tell us about neuronal activity?. *Nat. Rev. Neurosci.* **3**, 142–151 (2002).
81. Shmuel, A., Augath, M., Oeltermann, A. & Logothetis, N. K. Negative functional MRI response correlates with decreases in neuronal activity in monkey visual area V1. *Nat. Neurosci.* **9**, 569–577 (2006).
82. Harel, N., Lee, S. P., Nagaoka, T., Kim, D. S. & Kim, S. G. Origin of negative blood oxygenation level-dependent fMRI signals. *J. Cereb. Blood Flow. Metab.* **22**, 908–917 (2002).
83. Devor, A. et al. Suppressed neuronal activity and concurrent arteriolar vasoconstriction may explain negative blood oxygenation level-dependent signal. *J. Neurosci.* **27**, 4452–4459 (2007).

84. Gong, Z. Q. & Zuo, X. N. Dark brain energy: toward an integrative model of spontaneous slow oscillations. *Phys. Life Rev.* **52**, 278–297 (2025).
85. Marques, J. P. et al. MP2RAGE, a self bias-field corrected sequence for improved segmentation and T1-mapping at high field. *Neuroimage* **49**, 1271–1281 (2010).
86. Worsley, K. J. in *Functional Magnetic Resonance Imaging: an Introduction to Methods* (eds Peter Jezzard, Paul M. Matthews, & Stephen M. Smith) 251–270 (Oxford University Press, 2001).
87. Huber, L. R. et al. LayNii: a software suite for layer-fMRI. *Neuroimage* **237**, 118091 (2021).

Acknowledgements

This work was supported by IBS-R015-D1 (S.-G.K.) and IBS-R015-D2 (C.-W.W.) (Institute for Basic Science, Korea), 2016R1C1B2015901 (D.K.), RS-2023-00217361 (M.-S.K.) (National Research Foundation of Korea) and K411000 (S.H.H.) (Korea Basic Science Institute). We also thank Boohee Choi for data collection. The authors have no conflicts of interest to declare.

Author contributions

D.K, C.-W.W. and S.-G.K. designed the experiment. D.K., S.H.H., S.Y.K., and S.G.E. conducted the experiments. D.K. and S.H.H. analyzed data. D.K., S.H.H., M.-S.K., C.-W.W., and S.-G.K. wrote the manuscript.

Competing interests

The authors declare no competing interests.

Additional information

Supplementary information The online version contains supplementary material available at https://doi.org/10.1038/s41467-026-71842-w.

Correspondence and requests for materials should be addressed to Choong-Wan Woo or Seong-Gi Kim.

Peer review information *Nature Communications* thanks Akshay Jagadeesh, Esther Kuehn and the other anonymous reviewer(s) for their contribution to the peer review of this work. A peer review file is available.